## Title

Comparison of DSC-MRI post-processing techniques in predicting microvascular histopathology in patients newly diagnosed with GBM



## Journal

Journal of Magnetic Resonance Imaging, 38(2)

## ISSN

1053-1807

## Authors

Essock-Burns, Emma
Phillips, Joanna J
Molinaro, Annette M
et al.

## Publication Date

2013-08-01

## DOI

10.1002/jmri.23982

Peer reviewed

Published in final edited form as:
*J Magn Reson Imaging*. 2013 August ; 38(2): 388–400. doi:10.1002/jmri.23982.

# Comparison of DSC-MRI post-processing techniques in predicting microvascular histopathology in patients newly diagnosed with GBM

**Emma Essock-Burns, PhD**[1,2], **Joanna J. Phillips, MD**[3,4], **Annette M. Molinaro, PhD**[3,5], **Janine M. Lupo, PhD**[2], **Soonmee Cha, MD**[2,3], **Susan M. Chang, MD**[3], and **Sarah J. Nelson, PhD**[1,2,6]

[1]The UC Berkeley – UCSF Graduate Program in Bioengineering, University of California, San Francisco, San Francisco, CA, United States

[2]Department of Radiology and Biomedical Imaging, University of California, San Francisco, San Francisco, CA, United States

[3]Neurological Surgery, University of California, San Francisco, San Francisco, CA, United States

[4]Department of Pathology, University of California, San Francisco, San Francisco, CA, United States

[5]Epidemiology and Biostatistics, University of California, San Francisco, San Francisco, CA, United States

[6]Bioengineering and Therapeutic Sciences, University of California, San Francisco, San Francisco, CA, United States

## Abstract

**Purpose—**To evaluate which common post-processing method applied to gradient-echo DSC-MRI data, acquired with a single gadolinium injection and low flip-angle, most accurately reflects microvascular histopathology for patients with de novo, treatment-naive glioblastoma multiforme (GBM).

**Materials and Methods—**72 tissue samples were collected from 35 patients with treatment-naïve GBM. Sample locations were co-registered to preoperative gradient-echo dynamic susceptibility contrast (DSC) MRI acquired with 35° flip-angle and 0.1mmol/kg gadolinium. Estimates of blood volume and leakiness at each sample location were calculated using four common post-processing methods (leakage-corrected nonlinear gamma-variate, non-parametric, scaled MR-signal, and unscaled MR-signal). Tissue sample microvascular morphology was characterized using Factor VIII immunohistochemical analysis. A random-effects regression model, adjusted for repeated measures and contrast-enhancement, identified whether MR parameter estimates significantly predicted IHC findings.

**Results—**Elevated blood volume estimates from nonlinear and non-parametric methods significantly predicted increased microvascular hyperplasia. Abnormal microvasculature existed beyond the CE-lesion and was significantly reflected by increased blood volume from nonlinear, non-parametric, and scaled MR-signal analysis.

**Conclusion—**This study provides histopathological support for both non-parametric and nonlinear post-processing of low flip-angle DSC-MRI for characterizing microvascular

**Corresponding Author:** Emma Essock-Burns, Byers Hall Rm 303, Box # 2352, 1700 4th Street, University of California, San Francisco, San Francisco, CA 94158, Emma.essock-burns@ucsf.edu, (415) 514-4419 (phone), (415) 476-6022 (fax).

hyperplasia within GBM. Non-parametric analysis with a single gadolinium injection may be a particularly useful strategy clinically, as it requires less computational expense and limits gadolinium exposure.

**Keywords**

perfusion MRI; tissue sample; DSC post-processing; microvascular histopathology; low flip angle

## Introduction

Dynamic susceptibility-weighted contrast-enhanced (DSC) MR imaging is used for patients with brain tumors to noninvasively assess the tumor angiogenesis and underlying microvascular environment in the lesion and surrounding tissue. DSC MR imaging has become increasingly important in the management of patients with glioma as the therapy paradigm shifts to incorporate anti-angiogenic therapy. One of the challenges of assessing response in this context is that anti-angiogenic agents directly remove what has historically been considered the primary surrogate outcome measure for assessing treatment response, namely the presence of a contrast-enhancing lesion after the injection of a gadolinium based MR contrast agent (1,2). It is for this reason that DSC imaging has received increasing attention as a more quantitative method for evaluating microvascular changes associated with the tumor (3–5).

Gliomas are the most common malignant primary brain tumor in adults and are highly infiltrative in nature. Accurate diagnosis and definition of tumor grade is based upon histopathologic evaluation of tissue samples obtained by stereotactic biopsy or surgical resection using WHO criteria (6). Glioblastoma multiforme (GBM) is the most malignant and the highest grade glioma (Grade IV) and is characterized by increased cellular proliferation, nuclear atypia, necrosis and microvascular proliferation. Microvascular hallmarks of GBM include the presence of complex microvascular hyperplasia, epitomized by “glomeruloid” bodies, tortuous lamina, and breakdown of the blood brain barrier (BBB) (7). Histopathologic and immunohistochemical (IHC) analysis of the biopsy sample can be used to highlight the microvasculature and is the gold-standard for determining malignancy.

Noninvasive DSC imaging assesses vascular function by tracking the relaxation effects of injected gadolinium-based MR contrast agent as it circulates through the brain. Following the injection of a bolus of gadolinium, the observed T2 or T2*-weighted signal decreases and then recovers as the agent recirculates. The reduction in signal is due to spin-spin dephasing caused by the susceptibility gradient induced by the intravascular compartmentalized gadolinium (8). The changes in signal intensity can be modeled as a change in T2* relaxivity ($\Delta R_2^*$), which has a nearly linear relationship with contrast agent concentration and provides information about the hemodynamics of the tissue. A number of different parameters are computed from the concentration-time curve to create various parametric maps that reflect different characteristics of the underlying microvasculature in the tumor region. The most common parameter used to describe the changes in signal intensity is the relative cerebral blood volume (rCBV), which represents bulk vessel density often expressed as a ratio value to contralateral normal appearing white matter.

For regions where there is breakdown of the BBB, the extravasation of the contrast agent causes a change in the T1 relaxation time which modifies the observed signal intensity and makes the estimation of vascular parameters more complex (9). Multiple strategies have been proposed to address this situation (10–13). Acquisition methods to reduce the impact of the T1 effect include the use of a low flip angle (35°) gradient echo sequence (14,15), the implementation of a dual-echo sequence (16–18) and the application of an additional, pre-

load injection of gadolinium (10,19,20). A post-processing strategy that has been widely used in a research setting, is to model the $\Delta R_2^*$ curve as the sum of a gamma-variate function that results from the bolus and an additional component caused by leakage. This requires a more complex nonlinear fitting procedure to estimate model parameters such as rCBV and leakage factor (RF), but the resulting values been shown to correlate well with glioma grade (21).

In cases where a low flip angle is used for data acquisition, a simpler, non-parametric approach to characterizing the $\Delta R_2^*$ curve is the determination of the relative peak height (rPH) and percent signal recovery to baseline (PSR). Reduced rPH and PSR have been shown to differentiate brain metastasis from GBM (22). In patients newly diagnosed with GBM, the magnitude of PSR early in therapy was shown to be associated with progression-free survival (23). In a clinical setting, estimates of rCBV have also been calculated directly from the MR signal trace, either scaled to initial baseline levels (13) or unscaled raw MR data (12). These parameters require minimal computational time for post-processing the data, which makes them a common choice for use in the clinic, but there is limited evidence to support their relationship to physiologic variables (12).

The goal of this study was to apply the most common post-processing methods to DSC imaging data that were acquired with a single dose of gadolinium and a low flip angle using gradient-echo sequence in order to determine which method most accurately reflects the underlying vascular pathology for patients with de novo, treatment-naive GBM. This was achieved by acquiring DSC data from patients prior to surgical resection and making a direct comparison between MR parameter estimates from the locations where image guided tissue samples were obtained and the results from subsequent histopathological analysis of individual specimens.

## Materials and Methods

### Patient Population

Thirty-five patients with de novo (primary), treatment-naïve, pathologically confirmed GBM were included in this HIPPA compliant, imaging study. All patients received MRI exams, including anatomic and physiologic imaging, prior to undergoing tumor resection. Preoperative MR data were used to guide the site of tissue sample towards regions with elevated nCBV, low apparent diffusion coefficient (ADC), or high Choline-to-NAA index. Image-guided tissue samples were collected from these tumor locations and the MR imaging coordinates of the sample location were recorded using Brainlab software (Vector Vision Navigation System, Medtronic, Stealth Station). Once removed, the 5mm-diameter spherical samples (approximately 50 mg) were divided into two sections; half was snap-frozen and stored for ex vivo analysis (24) and half was fixed in 10% buffered formalin for histologic and immunohistologic evaluation. The tissue specimen handling methods have been described previously (25).

### MRI Protocol

MR imaging exams were performed on a 3T GE scanner and included both anatomic and physiologic imaging. In selected cases lactate edited $^1$H MRSI data were also collected using methods described previously (26,27) and used as an adjunct to the other measurements to select regions of putative tumor for targeting tissue collection. The standard anatomic imaging protocol included axial T2 weighted FLAIR sequence (TE= 120 ms, TR = 10,000 ms, TI = 2200 ms, slice thickness = 3mm, slice gap = 0 mm, matrix = 192×256, FOV = 24×24 cm) and pre- and post-contrast axial T1-weighted 3D IRSPGR (TE=2.5 ms, TR = 8.9 ms, TI = 400 ms, slice thickness = 1.5mm, matrix = 256×256, FOV =

24×24 $cm^2$ with acceleration factor R=2). The standard physiologic imaging included diffusion-weighted imaging (DWI) and DSC perfusion imaging. DWI was acquired with a 2D spin-echo, echo-planar sequence (TE = 99 ms, TR = 10,000 ms, slice thickness = 3mm, matrix = 256×256, FOV = 24×24 $cm^2$, 6 gradient directions, b=0 and 1000 $s/mm^2$). Gradient-echo, echo-planar DSC imaging (TE = 54 – 56 ms, TR = 1250 – 1500 ms, flip angle = 35°, slice thickness = 3–4 mm, matrix = 128 × 128, FOV = 24 × 24 $cm^2$) was acquired before, during, and following an injection of 0.1 mmol/kg gadolinium contrast agent (Magnevist, Bayer HealthCare Pharmaceuticals Inc.) at 4–5 ml/s. Fifteen seconds of dynamic imaging was acquired prior to the contrast agent injection. The first five data points acquired were excluded and the following 10 data points were used to get an estimate of baseline. Total DSC imaging time was 100 – 120 seconds. DSC was acquired with a gradient-echo pulse sequence and single dose of gadolinium in order to reduce the risks associated with additional gadolinium exposure. A flip-angle of 35° was chosen for all DSC acquisitions in this study in order to minimize T1 sensitivity during the first-pass of the contrast agent. A TE of 54–56 ms was selected to maximize the susceptibility change during the first-pass of contrast agent. These parameters have consistently achieved maximum contrast between normal appearing white matter and tumor during the recirculation phase of contrast at our institution.

## DSC Image-Processing

The DSC data were non-rigidly aligned to the pre-contrast, T1-weighted images using B-spline warping by maximization of normalized mutual information in order to minimize distortion from the echo-planar imaging (28,29). A 5-mm diameter spherical region of interest (ROI) was placed at the corresponding surgical coordinates of the image-guided target location on the co-registered MRI images (BrainLab, VectorVision Navigation System; Medtronic, Stealth Station). The region of normal-appearing white matter (NAWM) was defined semi-automatically on the pre-contrast T1-weighted image (27). These ROI's were then re-sampled to the native resolution of the DSC data set and overlaid on the DSC data at the original resolution. Average hemodynamic curves were calculated within each specimen region and NAWM using each of the 4 post-processing methods selected for comparison in this study. Any voxel with a signal peak of less than 4 times the baseline noise level was excluded to insure that necrosis voxels would not be included in the representative biopsy average curve. The four post-processing methods included: i) Nonlinear Fit Model of concentration-time curve (nl), (ii) Non-parametric concentration-time curve analysis (np), (iii) Scaled MR signal-time curve analysis (sc), and (iv) Unscaled MR signal-time curve analysis (unsc). Strategies (i) and (ii) are both commonly accepted in the research community (8,9,21,30), while strategies (iii) and (iv) are often used in the clinical setting (12,13). Table 1 describes the hemodynamic curve data, model, and derived parameters for each of these four methods and Figure 1 illustrates examples of the derived perfusion parameters.

These post-processing methods are described in two steps: (1) manipulation of the hemodynamic data curve and (2) calculation of derived parameters.

**Step 1. Manipulation of the Hemodynamic Data Curve—**Average DSC data were either (A) converted to change in relaxivity ($\Delta R_2^*$) representative of the concentration-time curve using Equation 1 or (B) left as MR signal-time curve.

$$\Delta R_2^* = -\frac{\ln(S_1(t) - S_0)}{TE} \quad \text{(Equation 1)}$$

**Step 2. Calculation of Derived Perfusion Parameters—**Perfusion parameters that were derived included estimates of blood volume (rCBV, peak height (PH), negative enhancement integral (NEI), or maximum signal drop (MSD)) and estimates of vessel leakiness (percent signal recovery (PSR)) depending on the post-processing method. The average hemodynamic curve from within NAWM was used as a normalization reference to compute normalized blood volume measures (nCBV, nPH, nNEI, nMSD, Figure 1).

**A.** $\Delta R_2^*$ Signal

**(i)** *Nonlinear Fit Model (nl):* The concentration-time curve was fit with a nonlinear gamma-variate model with leakage correction (9). nCBV(nl), nPH(nl), and PSR(nl) were calculated from the model of the first pass (Figure 1.i: Nonlinear Fit Model).

**(ii)** *Non-parametric Analysis (np):* The concentration-time curve was used to directly calculate nPH(np) and PSR(np), without fitting a parametric model (Figure 1.ii: Non-Parametric).

**B.** MR Signal

**(iii)** *Scaled MR Signal Analysis (sc)*: The $T_2^*$ MR signal intensity-time curve was scaled to baseline MR signal intensity (mean of the $5^{th}$ through $10^{th}$ time-points) and baseline was shifted to 1000 MR arbitrary units. nMSD(sc), nNEI(sc), and PSR(sc) were calculated from this scaled MR signal-time curve (see Figure 1.iii: Scaled MR Signal)

**(iv)** *Unscaled MR Signal Analysis (unsc):* The raw $T_2^*$ MR signal intensity-time curve was used to directly calculate nMSD(unsc), nNEI(unsc), and PSR(unsc) (Figure 1.iv: Unscaled MR Signal)

## Factor VIII Immunohistochemical Microvascular Staining

Immunohistochemistry for Factor VIII, rabbit polyclonal antibody (Dako) at 1.2 μg/ml for 20 min at 37°C, was analyzed blinded to the MRI findings by an experienced neuropathologist. On the basis of Factor VIII immunostaining, the microvascular morphology was graded as delicate (resembling normal cerebral vessels), simple microvascular hyperplasia (circumferential single cell hyperplasia with definitive lumen), or complex microvascular hyperplasia (circumferential multi-layered and glomeruloid-type vessels). Two features were scored from the factor VIII IHC results, (1) relative contribution of each vascular morphology and (2) overall vascular morphology score. The relative contribution of each vascular morphology to total vascularity within the sample was qualitatively measured on a four-tiered ordinal scale (0, no contribution; 1, minimal; 2, prevalent; 3, predominant) at a magnification of 200×. The overall microvascular morphology score assigned to each tissue sample corresponded to the most abnormal, morphologic-type of vasculature present in the sample as follows: 0, delicate only; 1, simple microvascular hyperplasia; and 2, complex microvascular hyperplasia. For example, samples that contained any contribution of complex hyperplasia were scored as “complex.” Whereas, samples that contained a mix of delicate and simple, but no complex vasculature, were scored as “simple.” Digital images were captured using a microscope (Olympus, Model BX41TF) and digital camera (Olympus, Model DP70).

## Contrast-Enhancing vs. Non-enhancing Classification of Specimens

Each tissue specimen ROI, in the native DSC resolution, was also overlaid on the T1-weighted post-contrast image in order to determine if the sample originated from a lesion

location with contrast-enhancement (CE) or no contrast-enhancement (NE). A board-certified radiologist evaluated all CE and NE classifications blinded to the DSC findings.

### Statistical Analysis

A random-effects regression model, adjusted for CE categorization at the specimen location and repeated specimen samples per patient, was used to determine if the perfusion parameters from each post-processing method significantly predicted IHC findings. The two types of factor VIII IHC findings, vascular morphology (delicate, simple, complex) and relative contribution of each vascular morphology (0-none to 3-large) were treated as ordinal outcomes on a 3-tiered and 4-tiered scale, respectively. Outcome levels were also grouped to assess whether DSC findings were predictive of complex vasculature (delicate or simple vs. complex) or abnormal vasculature (delicate vs. simple or complex). Binary CE categorization was included as a covariate in each model to adjust for CE at the specimen site, which is known to be associated with increased microvascular density and abnormal perfusion (31).

To assess the association of the perfusion parameters and the ordinal histopathology variables we employed a proportional odds logistic regression model with repeated measures to model the probability of observing a lower vs. a higher response. This model is written as:

$$\log it[P(Y_{ijk} \leq \kappa | X_i, Z_i)] = a_\kappa + x_{ij}^{'}\beta + z_{ij}^{'}b_i; i=1,\ldots,35; \kappa=1,\ldots,c-1 \quad \text{(Equation 2)}$$

where $c$ is the total number of levels of the ordinal variable, $X_i$ is the design matrix for the fixed effects and $Z_i$ for the random effects; $x_{ij}$ and $z_{ij}$ are rows corresponding to the $j$th biopsy specimen (ranges from 1 to 4); and β & $b_i$ are the vectors of fixed and random parameters. The intercepts are fixed and category dependent. The odds ratio and p-value for each variable is reported. The ordinal-valued outcome mixed effect models were analyzed with PROC GENMOD in SAS v.9.2.

Significance was assessed at $p<.05$ for all models. Due to the exploratory nature of the study, no adjustment for type I error was included. Any perfusion parameter that was predictive of IHC results at $p<.05$, adjusted for CE and repeated sampling, was deemed to be a significant predictor and is presented in the results. The method(s) with the greatest number of significant predictors was determined to be the post-processing method that most reflected underlying vascular histopathology.

## Results

### Tissue Specimen IHC Results

Table 2 summarizes the distribution of vascular morphology observed in the 72 samples obtained from the thirty-five patients with de-novo GBM. The number of samples acquired per patient ranged from 1 to 4 with an average of 2 samples per patient. Patient age ranged from 33 to 85 years old (median = 66) and 25 patients were male and 10 patients were female. 52 (72.2%) of the samples were from CE regions and 20 (27.8%) samples were from NE regions. The highest degree of microvascular hyperplasia within each sample was used to determine the overall microvascular morphology. Among the 72 samples, 16 contained at most delicate microvasculature (delicate), 27 contained at most simple microvascular hyperplasia (simple), and 29 contained complex microvascular hyperplasia (complex). As expected, the majority of complex hyperplasia was found in the CE specimens (89.6% of specimens with complex were CE), however approximately half of the CE specimens sampled did not contain complex microvascular hyperplasia.

## Predicting Vascular Morphology using DSC data

**Identification of Microvascular Morphology (delicate, simple, or complex)—** The ability of each post-processing method to predict the microvascular morphology of a tissue was further assessed using the proportional odds logistic regression statistical analysis. Odds ratios (OR) and significance of each regression model are reported in Table 3. Statistical results reflect each parameter adjusted for the other covariate in the model. For example, in the first model of nonlinear post-processing in Table 3 (shaded), the top row reports nCBV(nl) adjusted for presence of CE and the bottom row reports presence of CE adjusted for nCBV(nl) in predicting underlying vascular morphology.

The nCBV(nl), nPH(nl), and nPH(np) parameters significantly predicted the underlying vascular morphology ($p < 0.05$, $p = 0.02$, $p = 0.02$, respectively). The presence of CE, adjusted for blood volume, in each of these models was also a significant predictor of increasingly abnormal vascular morphology. This is expected since more samples with hyperplasia (simple or complex) were found in CE specimens than NE specimens (44 of 52 CE samples compared to 13 of 20 NE samples, Table 2). Perfusion parameters from scaled MR signal analysis and unscaled MR signal analysis were not predictive of vascular morphology (Table 3).

Figure 2 further illustrate the differences among post-processing methods in distinguishing between samples of different vascular morphologies. In Figure 2, histograms of a blood volume estimate from each of the four post-processing methods (a.–d.) are plotted grouped by the Factor VIII vascular morphology of the tissue samples. Samples with delicate microvasculature are shown in green, simple microvasculature are shown in blue, and samples with complex microvasculature are shown in red.

Note that for nonlinear and non-parametric analyses (Figure 2.a–b) samples with delicate microvasculature generally cluster at low blood volume (median nCBV(nl) = 1.79, median nPH(np) = 1.73), simple hyperplasia cluster in mid-range (median nCBV(nl) = 2.15, median nPH(np) = 1.98), and complex hyperplasia cluster in mid-to-high range (median nCBV(nl) = 2.55, median nPH(np) = 2.30). For scaled MR signal (Figure 2.c) the blood volume estimates of delicate microvasculature cluster in the low range (median nNEI(sc) = 1.78), but simple and complex show high overlap (median nNEI(sc) = 2.00 (simple), 2.07 (complex)). For unscaled MR signal (Figure 2.d), the blood volume estimates of samples with delicate, simple, and complex hyperplasia all show high overlap (median nNEI(unsc) = 2.72 (delicate), 3.04 (simple), 3.10 (complex)).

In general, a one-unit increase in the nonlinear and non-parametric blood volume measures corresponded to approximately 1.7 times increased likelihood of the sample containing microvasculature with a greater degree of hyperplasia (delicate, simple, complex; ORs in Table 3). Figure 3 illustrates how greater nCBV(nl), nPH(nl), and nPH(np) are predictive of increased microvascular hyperplasia present in the tissue sample.

**Identification of Complex Microvasculature—**The presence of CE was a highly significant covariate in the model predictor of complex hyperplasia in the tissue sample (CE presence covariate: $p<.05$ for each model, Table 4). Contrast enhancing biopsies were much more likely to contain complex microvascular hyperplasia (see high ORs in Table 4), as expected given greater contrast extravasation among markedly abnormal microvasculature. Even when adjusted for the presence of CE categorization, the nCBV(nl), nPH(nl), and nPH(np) were marginally significant risk factors for complex hyperplasia ($p=.09$, $p<.07$, $p<.08$ respectively, Table 4). Again, perfusion parameters derived from scaled MR signal analysis and unscaled MR signal analysis were not predictive of complex hyperplasia and neither were the PSR measures from any of the four post-processing methods (Table 4).

**Identification of Abnormal Microvasculature (Simple or Complex)—**The blood volume measures calculated from the nonlinear, non-parametric, and scaled MR signal methods each were significant predictors of the presence of abnormal microvasculature (simple or complex), while the presence of CE categorization was not (nCBV(nl): p=.03, nPH(nl): p<.03; nPH(np): p<.02; nNEI(sc): p<.03, nMSD(sc): p<.05; CE presence in each model: p≥.15). Unscaled MR signal analysis was not predictive of abnormal vasculature and neither were the PSR measures from any of the post-processing methods. 13 of the 20 NE specimens contained abnormal vasculature (simple = 10, complex = 3, Table 2). Table 5 describes the ORs and significance of each model in predicting abnormal microvasculature. Note that in Figure 2, this pattern of elevated blood volume in abnormal microvasculature (blue-simple and red-complex) compared to delicate microvasculature (green) is more evident in panels a – c (nonlinear, non-parametric, and scaled MR signal analysis), than in panel d (unscaled MR signal analysis).

In general, a 1-unit increase in the nonlinear, non-parametric, and scaled MR signal blood volume measures was associated with approximately a 2.3-fold greater likelihood of presence of abnormal microvasculature (ORs in Table 5). Figure 4 illustrates an example of a patient with abnormal microvasculature (simple or complex hyperplasia) in both the CE and NE tissue, which is reflected by elevated blood volume estimates from the nonlinear, non-parametric, and scaled MR signal analysis methods.

### Predicting Relative Contribution of Microvascular Morphology using DSC data

Based on immunostaining for Factor VIII the relative contribution of each microvascular pattern to the overall microvasculature, was similarly evaluated to determine if any of the DSC parameters were significant predictors. Adjusted for CE, nPH(nl) and nPH(np) were marginally significant predictors of a predominance of simple hyperplasia in the specimen (nPH(nl): OR = 1.42, p=.06; nPH(np): OR = 1.4, p=.06). In these models, presence of CE was a significant predictor of increased relative contribution of simple hyperplasia, with CE specimens more likely to contain a greater predominance of simple hyperplasia (p=.02, p=.03 respectively). Contrastingly, greater nPH(nl) and nPH(np) were not predictive of the predominance of complex hyperplasia. The perfusion parameters calculated from the scaled MR signal analysis and unscaled MR signal analysis were not found to be predictive of the relative contribution of any of the three vascular morphologies. Generally, perfusion parameters were found to better describe the type of microvascular hyperplasia present rather than relative extent of a given vascular morphology, which is described more thoroughly in the following discussion.

## Discussion

In this retrospective study, tissue samples were collected from patients with treatment-naïve GBM who had received a pre-operative MR imaging examination that included the acquisition of DSC data with a 35° flip angle and single-dose of gadolinium. Four common post-processing methods were applied to the DSC data and evaluated in order to determine whether any of the estimated perfusion parameters could non-invasively predict the underlying tissue microvasculature. It was found that blood volume measures from both the nonlinear and non-parametric analysis of the concentration time curve significantly predicted the underlying vascular morphology as defined by Factor VIII IHC analysis. Higher values of the nCBV and nPH obtained using the nonlinear fitting method and higher values of the non-parametric estimate of nPH were predictive of a greater degree of hyperplasia, both within the CE and the NE portion of the lesion.

Complex vasculature is a hallmark of GBM and more often present in specimens from the CE lesion. This is in agreement with previous research (13,31). However, not all CE-

specimens contained complex vasculature, implying that the tissue within this region has heterogeneous vascular morphology. The nonlinear and non-parametric DSC parameters may therefore assist in guiding sampling toward complex vasculature where it is present. There were only four patients who had a sample with complex vasculature that was represented as having lower blood volume than a sample with simple or delicate vasculature. In re-examining these cases, all four samples were removed from the central core of the CE-lesion or the internal edge of a contrast-enhancing rim around a necrotic core. Partial voluming of low signal from necrosis may have reduced the average hemodynamic curve from these ROIs. This suggests that care must be exercised in interpreting estimates of blood volume from regions that are close to necrosis.

Interestingly, while complex microvasculature was found preferentially in the CE lesion, simple microvasculature was found in specimens from the both the NE and CE lesion. Previous studies have shown abnormal, simple microvasculature to be associated with increased endothelial cellularity and luminal patency (32,33). In a complementary study investigating physiologic MRI correlates of histopathologic features within GBM, which included the patient cohort presented here, tissue samples with simple microvasculature were found to be associated with elevated cellularity, proliferation, and tumor score (25). The availability of a non-invasive method for identifying regions with abnormal microvascular hyperplasia that includes simple and complex morphologies is therefore key to characterizing vascular tumor burden, which often extends outside the CE lesion. Blood volume measures derived from the nonlinear, non-parametric, and scaled MR signal analyses were all able to identify abnormal vasculature, while the CE categorization did not. This suggests that CE alone is not sufficient in visualizing regions with abnormal microvasculature and that these DSC-derived blood volume measurements can identify abnormal microvascular morphology both within and beyond the CE lesion (example in Figure 4).

DSC perfusion parameters were more reflective of overall morphologic-type of microvasculature in the tissue sample than relative contribution of each vascular morphology within the sample. Both the nonlinear and non-parametric estimates of nPH were marginally predictive of the relative contribution of simple vasculature, while not predictive of the relative contribution of complex vasculature. This could be a limitation of the study since the relative contribution was a more qualitative parameter assessed from the IHC staining than the more general vascular morphology presence parameter. However, this could also reflect the nonlinearity of increasing relative contribution of complex vasculature and blood volume. Specimens with a high degree of complex, glomeruloid vasculature with partially thrombosed or minimally patent vessels may result in slower arrival of gadolinium or greater contrast agent extravasation, which may lead to reduced blood volume measures. Generally, these results support that the MR estimates of blood volume are more predictive of the dominant morphologic-type of microvasculature present in the sample location, rather than relative contribution of each specific vascular morphology.

The blood volume measurements calculated in this study were more predictive of vascular morphology rather than quantitative assessment of endothelial leakiness. Elevated blood volume may be more characteristic of specific abnormal vascular morphology, while leakiness measures, like PSR, may be more reflective of a combination of vascular type and amount of extravasation within the tissue microenvironment. Blood volume measures from non-parametric and nonlinear analysis were consistently reflective of underlying vasculature; observed through predicting morphology, identifying abnormal vasculature, and highlighting complex vasculature within the CE lesion. Scaled MR signal analysis was only found to be predictive of identifying abnormal vasculature, while the unscaled MR signal analysis was not found to be predictive of any of the IHC results.

One limitation of this study is the potential for misregistration between the tissue specimen location acquired with the surgical navigation tool and the pre-operative MR images due to tissue-shift during craniotomy. Multiple steps were taken during surgery to minimize this risk, such as avoiding substantial loss of cerebrospinal fluid, accurately registering imaging to patient's facial anatomy, and watching for brain swelling. In addition, by generating sufficiently large spherical ROI's (diameter of 5mm) representative of the tissue sample (approximately 50 mg) and resampling these to the native perfusion resolution, we attempted to compensate for any tissue shift at the specimen location. Thus, while both surgical and image analysis steps were taken to minimize this risk, there is still a possibility that the correspondence is imperfect.

Contrast-agent extravasation near areas of compromised BBB leads to competing signal enhancement, which is a known challenge that plagues interpretation of DSC perfusion parameters (9,10,21). Multiple acquisition strategies and post-processing methods exist for addressing this limitation and have been shown to greatly influence the resultant estimates of CBV (10). The acquisition strategy chosen for this study was a 35° flip angle to limit T1-sensitivity, a TE of 54–56 ms to maximize susceptibility contrast, and a single-dose of gadolinium to limit gadolinium exposure for patients. Of the 4 most common post-processing techniques compared, nonlinear and non-parametric analysis were consistently predictive of vascular morphology. Nonlinear gamma-variate fit with leakage correction, while a common method for addressing this extravasation limitation in the research setting, necessitates curve-fitting which limits its use in the clinical practice. Non-parametric analysis, which was equally representative of histopathology, is less computationally expensive and may be a better alternative for CBV estimation in the clinical setting. Both the scaled and unscaled MR signal analysis, which are often used in the clinical setting due to their direct ease of use, were not found to be predictive of vascular morphology. This highlights the need for an alternative post-processing method for DSC data that is histopathologically validated and easy-to-use in clinical practice. An open-source, freely available software package with non-parametric DSC post-processing analysis is currently being developed (34) such that these non-invasive blood volume measures can be used more reliably in clinical practice.

In conclusion, this study provides histopathological support for using both non-parametric and nonlinear post-processing techniques in conjunction with low flip angle DSC imaging data as noninvasive methods for characterizing microvascular hyperplasia within GBM. The non-parametric analysis method and acquisition strategy that requires a single injection of a standard dose of gadolinium may be particularly useful in the clinic, as it requires less computational expense and limits the potential side effects associated with gadolinium. The findings from this study also suggest that blood volume measurements derived in the manner described may assist in both guiding sites of tissue sampling to regions with vascular features characteristic of GBM and in identifying and monitoring patients with highly vascular GBM who may benefit from targeted antiangiogenic therapy.

## Acknowledgments

**Grant Support:** NIH Grant R01 CA127612-0A, NIH Grant P01 CA11816-01A2, NIH Grant K08 NS063456, and Howard Hughes Med Inst. #56006771

## References

1. Chang SM, Lamborn KR, Kuhn JG, et al. Neurooncology clinical trial design for targeted therapies: lessons learned from the North American Brain Tumor Consortium. Neuro-oncology. 2008; 10(4): 631–642. [PubMed: 18559968]

2. Wen PY, Macdonald DR, Reardon DA, et al. Updated response assessment criteria for high-grade gliomas: response assessment in neuro-oncology working group. J Clin Oncol. 2010; 28(11):1963–1972. [PubMed: 20231676]

3. Cha S, Tihan T, Crawford F, et al. Differentiation of low-grade oligodendrogliomas from low-grade astrocytomas by using quantitative blood-volume measurements derived from dynamic susceptibility contrast-enhanced MR imaging. AJNR Am J Neuroradiol. 2005; 26(2):266–273. [PubMed: 15709123]

4. Saito T, Yamasaki F, Kajiwara Y, et al. Role of perfusion-weighted imaging at 3T in the histopathological differentiation between astrocytic and oligodendroglial tumors. Eur J Radiol. [published online ahead of print May 2, 2011] PMID: 21543173 [PubMed - as suplied by publisher].

5. Nelson SJ. Assessment of therapeutic response and treatment planning for brain tumors using metabolic and physiological MRI. NMR Biomed. 2011; 24(6):734–749. [PubMed: 21538632]

6. Fuller GN, Scheithauer BW. The 2007 Revised World Health Organization (WHO) Classification of Tumours of the Central Nervous System: newly codified entities. Brain Pathol. 2007; 17(3):304–307. [PubMed: 17598822]

7. Rojiani AM, Dorovini-Zis K. Glomeruloid vascular structures in glioblastoma multiforme: an immunohistochemical and ultrastructural study. J Neurosurg. 1996; 85(6):1078–1084. [PubMed: 8929498]

8. Rosen BR, Belliveau JW, Vevea JM, Brady TJ. Perfusion imaging with NMR contrast agents. Magn Reson Med. 1990; 14(2):249–265. [PubMed: 2345506]

9. Weisskoff, RM. Simultaneous blood volume and permeability mapping using a single GD-based contrast injection. Proceedings of the 2nd Annual Meeting of ISMRM; San Francisco: 279. 1994.

10. Paulson ES, Schmainda KM. Comparison of dynamic susceptibility-weighted contrast-enhanced MR methods: recommendations for measuring relative cerebral blood volume in brain tumors. Radiology. 2008; 249(2):601–613. [PubMed: 18780827]

11. Lupo JM, Cha S, Chang SM, Nelson SJ. Dynamic susceptibility-weighted perfusion imaging of high-grade gliomas: characterization of spatial heterogeneity. AJNR American journal of neuroradiology. 2005; 26(6):1446–1454. [PubMed: 15956514]

12. Cha S, Lu S, Johnson G, Knopp EA. Dynamic susceptibility contrast MR imaging: correlation of signal intensity changes with cerebral blood volume measurements. J Magn Reson Imaging. 2000; 11(2):114–119. [PubMed: 10713942]

13. Barajas RF Jr, Hodgson JG, Chang JS, et al. Glioblastoma multiforme regional genetic and cellular expression patterns: influence on anatomic and physiologic MR imaging. Radiology. 2010; 254(2):564–576. [PubMed: 20093527]

14. Law M, Meltzer DE, Wetzel SG, et al. Conventional MR imaging with simultaneous measurements of cerebral blood volume and vascular permeability in ganglioglioma. Magn Reson Imaging. 2004; 22(5):599–606. [PubMed: 15172052]

15. Lee MC, Cha S, Chang SM, Nelson SJ. Dynamic susceptibility contrast perfusion imaging of radiation effects in normal-appearing brain tissue: changes in the first-pass and recirculation phases. J Magn Reson Imaging. 2005; 21(6):683–693. [PubMed: 15906330]

16. Heiland S, Benner T, Debus J, Rempp K, Reith W, Sartor K. Simultaneous assessment of cerebral hemodynamics and contrast agent uptake in lesions with disrupted blood-brain-barrier. Magn Reson Imaging. 1999; 17(1):21–27. [PubMed: 9888395]

17. Vonken EP, van Osch MJ, Bakker CJ, Viergever MA. Simultaneous quantitative cerebral perfusion and Gd-DTPA extravasation measurement with dual-echo dynamic susceptibility contrast MRI. Magn Reson Med. 2000; 43(6):820–827. [PubMed: 10861876]

18. Uematsu H, Maeda M, Sadato N, et al. Blood volume of gliomas determined by double-echo dynamic perfusion-weighted MR imaging: a preliminary study. AJNR Am J Neuroradiol. 2001; 22(10):1915–1919. [PubMed: 11733325]

19. Hu LS, Baxter LC, Smith KA, et al. Relative cerebral blood volume values to differentiate high-grade glioma recurrence from posttreatment radiation effect: direct correlation between image-guided tissue histopathology and localized dynamic susceptibility-weighted contrast-enhanced

perfusion MR imaging measurements. AJNR Am J Neuroradiol. 2009; 30(3):552–558. [PubMed: 19056837]

20. Hu LS, Baxter LC, Pinnaduwage DS, et al. Optimized preload leakage-correction methods to improve the diagnostic accuracy of dynamic susceptibility-weighted contrast-enhanced perfusion MR imaging in posttreatment gliomas. AJNR Am J Neuroradiol. 2010; 31(1):40–48. [PubMed: 19749223]
21. Boxerman JL, Schmainda KM, Weisskoff RM. Relative cerebral blood volume maps corrected for contrast agent extravasation significantly correlate with glioma tumor grade, whereas uncorrected maps do not. AJNR Am J Neuroradiol. 2006; 27(4):859–867. [PubMed: 16611779]
22. Cha S, Lupo JM, Chen MH, et al. Differentiation of glioblastoma multiforme and single brain metastasis by peak height and percentage of signal intensity recovery derived from dynamic susceptibility-weighted contrast-enhanced perfusion MR imaging. AJNR Am J Neuroradiol. 2007; 28(6):1078–1084. [PubMed: 17569962]
23. Essock-Burns E, Lupo JM, Cha S, et al. Assessment of perfusion MRI-derived parameters in evaluating and predicting response to antiangiogenic therapy in patients with newly diagnosed glioblastoma. Neuro-oncology. 2011; 13(1):119–131. [PubMed: 21036812]
24. Elkhaled AJL, Phillips JJ, et al. Magnetic resonance of 2-hydroxyglutarate in IDH1-mutated low-grade gliomas. Sci Transl Med. 2012; 4(116ra5)
25. Barajas RF Jr, Phillips JJ, Parvataneni R, et al. Regional variation in histopathologic features of tumor specimens from treatment-naive glioblastoma correlates with anatomic and physiologic MR Imaging. Neuro-oncology. 2012; 14(7):942–954. [PubMed: 22711606]
26. Crawford FW, Khayal IS, McGue C, et al. Relationship of pre-surgery metabolic and physiological MR imaging parameters to survival for patients with untreated GBM. J Neurooncol. 2009; 91(3): 337–351. [PubMed: 19009235]
27. Saraswathy S, Crawford FW, Lamborn KR, et al. Evaluation of MR markers that predict survival in patients with newly diagnosed GBM prior to adjuvant therapy. J Neurooncol. 2009; 91(1):69–81. [PubMed: 18810326]
28. Studholme CHD, Hawkes D. An overlap invariant entropy measure of 3D medical image alignment. Pattern Recognition. 1999; 3:16.
29. Rueckert D, Sonoda LI, Hayes C, Hill DL, Leach MO, Hawkes DJ. Nonrigid registration using free-form deformations: application to breast MR images. IEEE Trans Med Imaging. 1999; 18(8): 712–721. [PubMed: 10534053]
30. Lupo JM, Cha S, Chang SM, Nelson SJ. Analysis of metabolic indices in regions of abnormal perfusion in patients with high-grade glioma. AJNR Am J Neuroradiol. 2007; 28(8):1455–1461. [PubMed: 17846190]
31. Jain R, Narang J, Gutierrez J, et al. Correlation of immunohistologic and perfusion vascular parameters with MR contrast enhancement using image-guided biopsy specimens in gliomas. Acad Radiol. 2011; 18(8):955–962. [PubMed: 21718954]
32. Miyagami M, Katayama Y. Angiogenesis of glioma: evaluation of ultrastructural characteristics of microvessels and tubular bodies (Weibel-Palade) in endothelial cells and immunohistochemical findings with VEGF and p53 protein. Med Mol Morphol. 2005; 38(1):36–42. [PubMed: 16158178]
33. Izycka-Swieszewska E. [Immunomorphological analysis of the vascular stroma in glioblastoma]. Neurol Neurochir Pol. 2003; 37(1):59–71. [PubMed: 12910830]
34. Crane, JCOM.; Essock-Burns, E.; Lupo, JM.; Nelson, SJ. Visualization and Analysis of Dynamic MRSI and Perfusion MRI Using the Open-Source SIVIC Software Framework. 97th Annual meeting of RSNA; Chicago, IL. 2011. (Exhibit LL-INE1174)

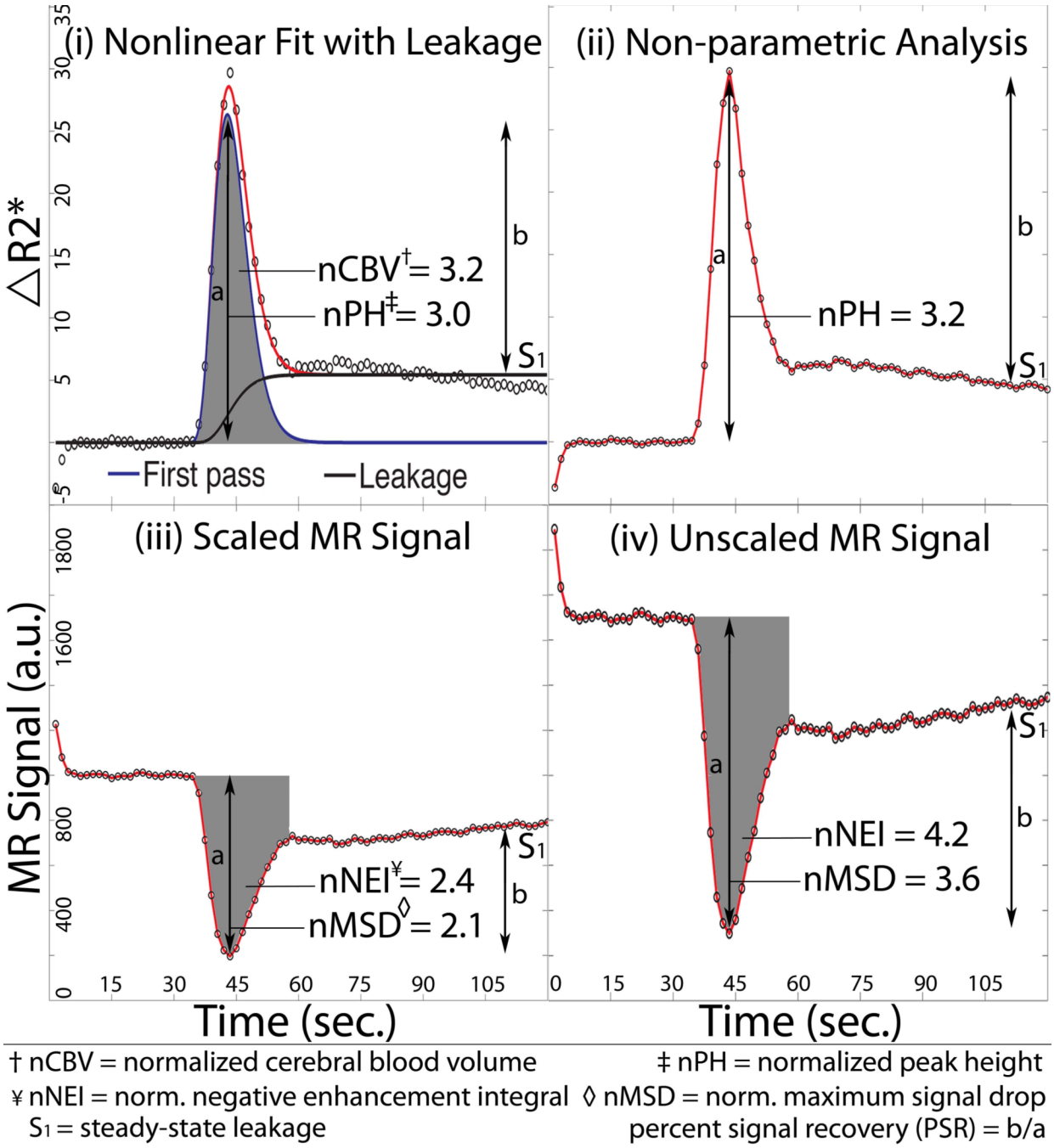


**Figure 1. Post-processing Methods**

Figure 1 illustrates the hemodynamic curve from a single CE-biopsy with complex vasculature calculated using each of the four post-processing methods. The first 5 data points were excluded from parameter calculation to allow for steady-state relaxation to be reached. All blood volume estimates were normalized to the respective blood volume estimate from the normal-appearing white matter (NAWM) hemodynamic curve to generate relative measures (nCBV, nPH, nNEI, nMSD, as marked in figure).

(i) Nonlinear gamma-variate fit with leakage correction (black curve) is used to calculate the leakage-corrected first-pass (blue curve) from the average $\Delta R_2^*$ data (black circles) within the

biopsy region. Peak height (PH) = peak of the first pass, cerebral blood volume (CBV) = integral of the first pass and S1 = steady-state height of the leakage component. Percent signal recovery (PSR) = b / a, where b = (PH – S1) and a = PH.

(ii) Non-parametric analysis is used to calculate the hemodynamic curve (red) directly from the average $\Delta R_2^*$ data (black circles) in the biopsy region. PH = maximum of the average hemodynamic curve and S1 = average of the last 15 time points acquired. PSR = b / a, where b = PH – S1 and a = PH.

(iii) Scaled MR signal analysis is used to scale the T2* signal intensity to the original baseline level and shift to 1000 MR au. Negative enhancement integral (NEI) is calculated using trapezoidal integration of signal-time curve from initial drop of signal to 3/2*full-width half-max of the first pass, maximum signal drop (MSD) = absolute value of the difference between the minimum of signal-time curve and the baseline average of $5^{th}$ through $15^{th}$ time-points, S1 = average of the last 15 time-points. PSR = b / a, where b = absolute value of the difference between the minimum of the signal-time curve and S1 and a = MSD.

(iv) Unscaled MR signal analysis is used to directly calculate perfusion parameters from the raw MR signal-time curve. NEI = trapezoidal integration of signal-time curve from initial signal drop to 3/2 * full-width half-max of the first pass, MSD = absolute value of the difference between the minimum of signal-time curve and the baseline average of $5^{th}$ through $15^{th}$ time-point and S1 = average of the last 15 time-points. PSR = b / a, where b = absolute value of the difference between the minimum of the signal-time curve and S1 and a = MSD.

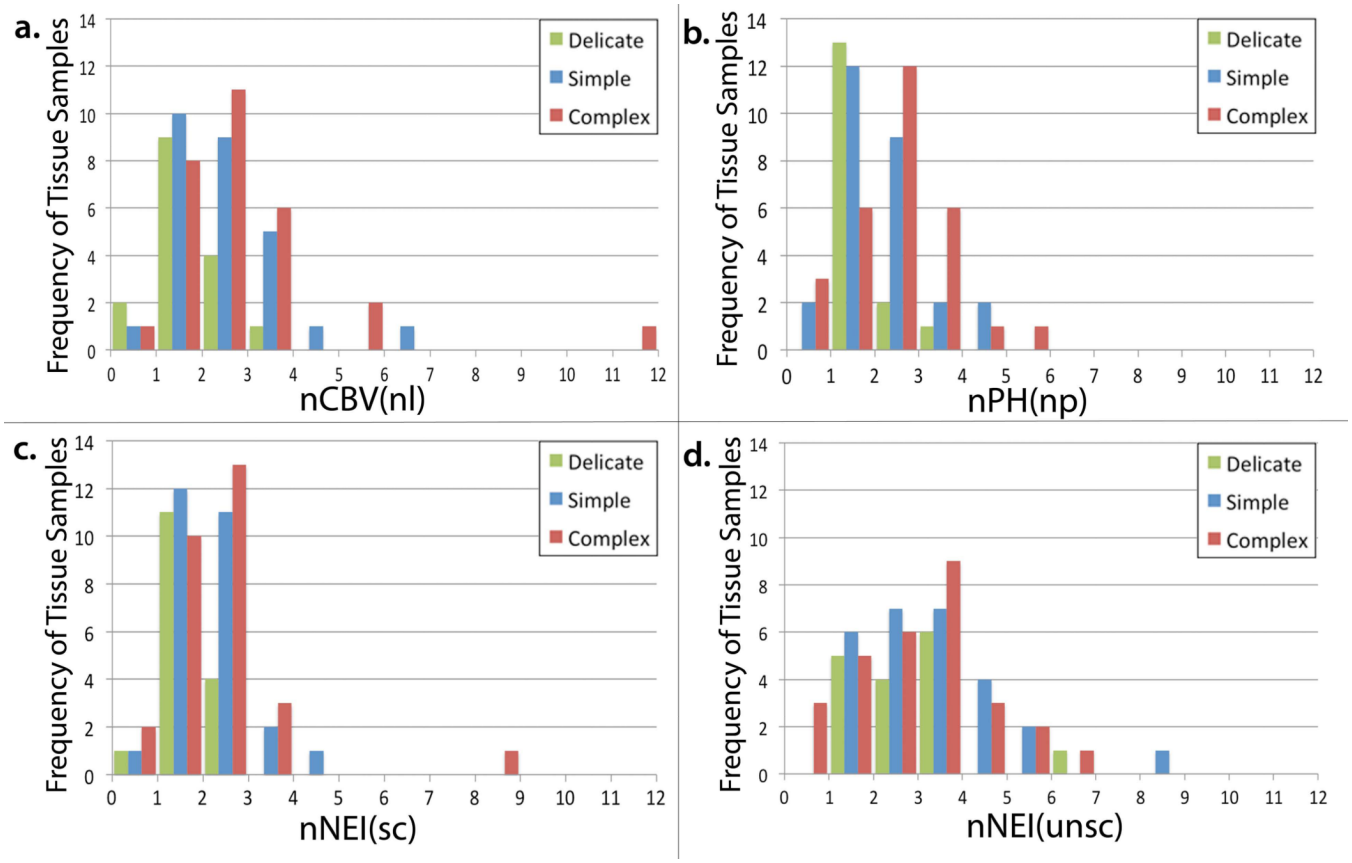


**Figure 2. Blood Volume Estimate and Microvascular Hyperplasia of Tissue Samples by Post-Processing Method**

Histograms illustrating the distribution of a blood volume estimate calculated from each of the four post-processing strategies within tissue samples of different vascular morphologies. DSC estimates of blood volume include: (a) nCBV(nl), (b) nPH(np), (c) nNEI(sc), and (d) nNEI(unsc). Samples with microvasculature classified as delicate are green, simple are blue, and complex are red. nCBV(nl) (a) and nPH(np) (b) show a more separable pattern between delicate (low-range), simple (mid-range) and complex (mid-to-high range) blood volume. nCBV(nl) (a), nPH(np) (b), and nNEI(sc) (c) show a separable pattern between delicate microvasculature samples (green) and abnormal microvasculature (simple-blue or complex-red) samples, whereas nNEI(unsc) shows high overlap among all vascular morphologies (d).

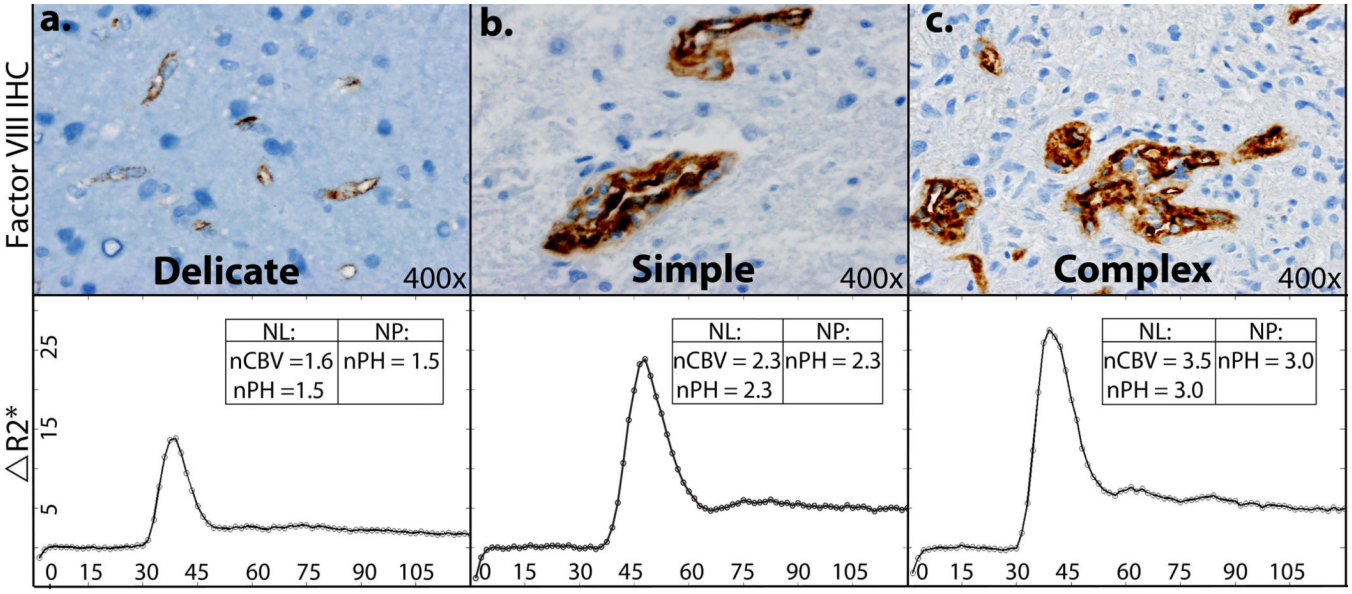


**Figure 3. Increasing blood volume measures from nonlinear and non-parametric analysis predict increasingly abnormal microvascular morphology.**

IHC staining (top) and corresponding $\Delta R_2^*$ curve (bottom) of 3 specimens with delicate, simple, and complex microvascular hyperplasia (a–c). Increased nCBV(nl), nPH(nl), and nPH(np) are significant risk factors for increased microvascular hyperplasia.

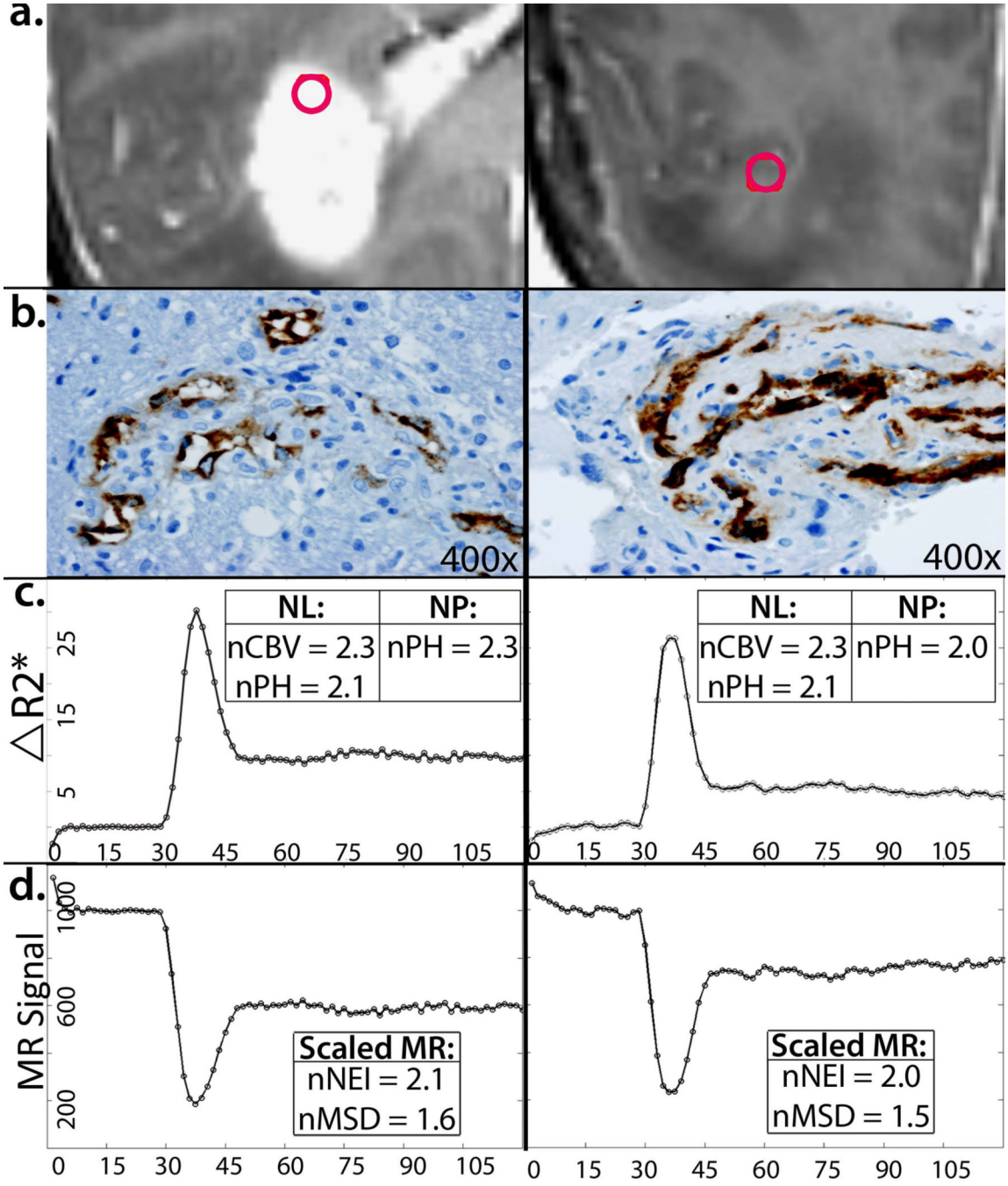


**Figure 4. Abnormal microvasculature detected by blood volume measures from nonlinear and non-parametric analysis, but not CE categorization.**

T1-weighted, post-contrast MRI of a patient with two tissue samples (a), one in the CE lesion (left) and one in the NE lesion (right). Factor VIII IHC staining demonstrates abnormal microvasculature (simple or complex hyperplasia) in both samples (b), which is reflected by elevated nCBV(nl), nPH (nl), and nPH(np) (c) as well as elevated nNEI(sc) and nMSD(sc) (d). Elevated blood volume estimates from nonlinear, non-parametric, and scaled MR signal post-processing methods detect abnormal hyperplasia within and beyond the CE-lesion.

## Table 1

### Post-processing methods and derived perfusion parameters

Table 1 describes the four post-processing methods compared in this study and the derived perfusion parameters. In step 1, the nonlinear and non-parametric analysis methods convert MR signal to $\Delta R_2^*$-time curve using Equation 1, while scaled MR signal and unscaled MR signal analysis methods do not. In step 2, the derived blood volume measures and leakiness measures for each method are named as shown.

| | | Post-Processing Methods & Derived Perfusion Parameters | | | |
|---|---|---|---|---|---|
| | | **Nonlinear** | **Non-parametric** | **Scaled MR signal** | **UnScaled MR signal** |
| **Step 1.** Manipulation of the hemodynamic data | | ΔR2*-time curve (Eq. 1) | | MR signal-time curve | |
| **Step 2.** Calculation of derived perfusion parameters | **Blood Volume Measures** | nCBV, nPH | nPH | nNEI, nMSD | nNEI, nMSD |
| | **Leakiness Measures** | PSR | PSR | PSR | PSR |

nCBV = normalized relative cerebral blood volume
nPH = normalized peak height
nMSD = normalized maximum signal drop
nNEI = normalized negative enhancement integral
PSR = percent signal recovery

## Table 2

**Distribution of biopsy specimens, vascular morphology and CE/NE classification.**

Table 2 details the distribution of biopsy specimens among the three vascular morphology levels within both the CE and NE lesion. There were 52 specimens from CE lesions and 20 specimens from NE lesions. The vast majority of complex vasculature was found in CE tissue samples (26 of 29 samples), yet approximately half of the CE samples did not contain complex vasculature, highlighting the heterogeneous nature of the CE lesion. Also note that 27 of the total samples contained simple vasculature, yet these were split between both the CE (17 samples) and NE lesion (10 samples).

| | Delicate: | Simple: | Complex: | Total: |
|---|---|---|---|---|
| **CE:** | 9 | 17 | 26 | 52 (72.2%) |
| **NE:** | 7 | 10 | 3 | 20 (27.8%) |
| **Total:** | 16 (22.2%) | 27 (37.5%) | 29 (40.3%) | 72 Specimens |

CE = Contrast-enhancement
NE = No contrast-enhancement

## Table 3

**Mixed Effects Model Results: DSC Perfusion Parameters in Predicting Microvascular Morphology (Delicate, Simple, Complex) by Post-Processing Method.**

Table 3 displays the mixed effects regression model results of predicting microvascular morphology based on MRI data. Results are grouped by DSC post-processing method (left column) and the alternating shading delineates the individual multi-variate models. Statistical models include two covariates: the DSC-derived perfusion parameter (top row) and the binary presence of contrast-enhancement (CE, bottom row). Statistical results reflect each parameter adjusted for the other covariate in the model. Note blood volume measures from nonlinear analysis and non-parametric analysis significantly predict vascular morphology, while the other post-processing methods do not.

| Statistical Results: Predicting Microvascular Morphology (Delicate vs Simple vs Complex) | | | | |
|---|---|---|---|---|
| **Post-Processing Method** | **Parameter** | **Odds Ratio** | **95% Confidence Interval** | **p-value** |
| Nonlinear | nCBV(nl) | 1.578 | [1.010, 2.466] | 0.045* |
| | CE Presence | 3.490 | [1.253, 9.716] | 0.016* |
| | nPH(nl) | 1.757 | [1.084, 2.848] | 0.022* |
| | CE Presence | 3.934 | [1.407, 11.000] | 0.009* |
| | PSR(nl) | 1.004 | [0.978, 1.030] | 0.790 |
| | CE Presence | 3.928 | [1.333, 11.574] | 0.013* |
| Non-Parametric | nPH(np) | 1.717 | [1.0751, 2.743] | 0.024* |
| | CE Presence | 3.702 | [1.314, 10.428] | 0.013* |
| | PSR(np) | 1.004 | [0.966, 1.043] | 0.843 |
| | CE Presence | 3.871 | [1.324, 11.318] | 0.013* |
| Scaled MR Signal | nNEI(sc) | 1.675 | [0.914, 3.070] | 0.095 |
| | CE Presence | 3.196 | [1.114, 9.171] | 0.031* |
| | nMSD(sc) | 1.910 | [0.728, 5.015] | 0.189 |
| | CE Presence | 3.505 | [1.223, 10.044] | 0.020* |
| | PSR(sc) | 0.991 | [0.957, 1.027] | 0.627 |
| | CE Presence | 3.152 | [1.098, 9.054] | 0.033* |
| Unscaled MR Signal | nNEI(unsc) | 0.996 | [0.719, 1.382] | 0.983 |
| | CE Presence | 3.658 | [1.199, 11.167] | 0.023* |
| | nMSD(unsc) | 0.907 | [0.614, 1.338] | 0.621 |
| | CE Presence | 3.652 | [1.195, 11.165] | 0.023* |
| | PSR(unsc) | 0.992 | [0.959, 1.025] | 0.621 |
| | CE Presence | 3.162 | [1.096, 9.124] | 0.033* |

nl = nonlinear
np = non-parametric
sc = scaled MR signal
unsc = unscaled MR signal
CE = contrast-enhancement
nCBV = normalized cerebral blood volume
nPH = normalized peak height

PSR = percent signal recovery
nNEI = normalized negative enhancement integral
nMSD = normalized maximum signal decrease

* p<.05

## Table 4

**Mixed Effects Model Results: DSC Perfusion Parameters in Predicting Complex Microvasculature by Post-Processing Method.**

Table 4 displays the mixed effects regression model results of predicting complex microvasculature in the tissue sample based on MRI data. Results are grouped by DSC post-processing method (left column) and the alternating shading delineates the individual multivariate models. Statistical models include two covariates: the DSC-derived perfusion parameter (top row) and the binary presence of contrast-enhancement (CE, bottom row Statistical results reflect each parameter adjusted for the other covariate in the model. Presence of CE is a strong predictor of complex vasculature, as expected given greater extravasation near markedly abnormal vessels with complex hyperplasia, with an odds ratio of approximately 6 across the analysis methods. Interestingly, even adjusted for presence of CE, nCBV(nl), nPH(nl) and nPH(np) are marginally significant predictors of complex hyperplasia.

| Statistical Results Predicting Complex Microvasculature | | | | |
|---|---|---|---|---|
| **Post-Processing Method** | **Parameter** | **Odds Ratio** | **95% Confidence Interval** | **p-value** |
| Nonlinear | nCBV(nl) | 1.515 | [0.933, 2.458] | 0.093 |
| | CE Presence | 5.583 | [1.567, 19.89] | 0.008* |
| | nPH(nl) | 1.651 | [0.967, 2.820] | 0.066 |
| | CE Presence | 6.236 | [1.739, 22.361] | 0.005* |
| | PSR(nl) | 1.002 | [0.977, 1.028] | 0.872 |
| | CE Presence | 5.924 | [1.461, 24.023] | 0.013* |
| Non-Parametric | nPH(np) | 1.607 | [0.946, 2.731] | 0.079 |
| | CE Presence | 5.891 | [1.620, 21.413] | 0.007* |
| | PSR(np) | 1.002 | [0.966, 1.039] | 0.910 |
| | CE Presence | 5.857 | 1.446, 23.717] | 0.013* |
| Scaled MR Signal | nNEI(sc) | 1.564 | [0.814, 3.006] | 0.179 |
| | CE Presence | 5.062 | [1.350, 18.980] | 0.016* |
| | nMSD(sc) | 1.658 | [0.568, 4.842] | 0.355 |
| | CE Presence | 5.438 | [1.442, 20.506] | 0.012* |
| | PSR(sc) | 0.993 | [0.960, 1.027] | 0.681 |
| | CE Presence | 4.973 | [1.167, 21.194] | 0.030* |
| Unscaled MR Signal | nNEI(unsc) | 0.926 | [0.636, 1.348] | 0.688 |
| | CE Presence | 5.779 | [1.415, 23.608] | 0.015* |
| | nMSD(unsc) | 0.809 | [0.513, 1.276] | 0.362 |
| | CE Presence | 5.703 | [1.418, 22.931] | 0.014* |
| | PSR(unsc) | 0.994 | [0.962, 1.027] | 0.717 |
| | CE Presence | 5.060 | [1.199, 21.351] | 0.027* |

nl = nonlinear
np = non-parametric
sc = scaled MR signal
unsc = unscaled MR signal
CE = contrast-enhancement

nCBV = normalized cerebral blood volume
nPH = normalized peak height
PSR = percent signal recovery
nNEI = normalized negative enhancement integral
nMSD = normalized maximum signal decrease

* $p<.05$

## Table 5

### Mixed Effects Model Results: DSC Perfusion Parameters in Predicting Abnormal Microvasculature (Simple or Complex) by Post-Processing Method

Table 5 displays the mixed effects regression model results of predicting abnormal microvasculature (simple or complex) in the tissue sample based on MRI data. Results are grouped by DSC post-processing method (left column) and the alternating shading delineates the individual multi-variate models. Statistical models include two covariates: the DSC-derived perfusion parameter (top row) and the binary presence of contrast-enhancement (CE, bottom row). Statistical results reflect each parameter adjusted for the other covariate in the model. Blood volume measures derived from nonlinear analysis, non-parametric analysis, and scaled MR signal analysis each significantly predict abnormal vasculature, while presence of CE does not.

| Statistical Results: Predicting Abnormal Microvasculature (Simple or Complex) | | | | |
|---|---|---|---|---|
| **Post-Processing Method** | **Parameter** | **Odds Ratio** | **95% Confidence Interval** | **p-value** |
| Nonlinear | nCBV(nl) | 1.993 | [1.054, 3.766] | 0.034 * |
| | CE Presence | 2.369 | [0.611, 9.183] | 0.212 |
| | nPH(nl) | 2.200 | [1.096, 4.416] | 0.027 * |
| | CE Presence | 2.720 | [0.693, 10.670] | 0.151 |
| | PSR(nl) | 1.009 | [0.981, 1.037] | 0.540 |
| | CE Presence | 3.127 | [0.769, 12.710] | 0.111 |
| Non-Parametric | nPH(np) | 2.232 | [1.182, 4.214] | 0.013 * |
| | CE Presence | 2.495 | [0.644, 9.658] | 0.186 |
| | PSR(np) | 1.012 | [0.969, 1.057] | 0.597 |
| | CE Presence | 3.124 | [0.770, 12.673] | 0.111 |
| Scaled MR Signal | nNEI(sc) | 2.282 | [1.100, 4.733] | 0.027 * |
| | CE Presence | 2.145 | [0.553, 8.316] | 0.270 |
| | nMSD(sc) | 2.942 | [1.041, 8.313] | 0.042 * |
| | CE Presence | 2.462 | [0.623, 9.723] | 0.199 |
| | PSR(sc) | 0.995 | [0.955, 1.035] | 0.791 |
| | CE Presence | 2.331 | [0.657, 8.271] | 0.190 |
| Unscaled MR Signal | nNEI(unsc) | 1.122 | [0.765, 1.647] | 0.556 |
| | CE Presence | 2.526 | [0.620, 10.283] | 0.196 |
| | nMSD(unsc) | 1.074 | [0.670, 1.720] | 0.768 |
| | CE Presence | 2.581 | [0.625, 10.663] | 0.190 |
| | PSR(unsc) | 0.993 | [0.957, 1.031] | 0.719 |
| | CE Presence | 2.268 | [0.636, 8.091] | 0.207 |

nl = nonlinear
np = non-parametric
sc = scaled MR signal
unsc = unscaled MR signal
CE = contrast-enhancement
nCBV = normalized cerebral blood volume
nPH = normalized peak height
PSR = percent signal recovery
nNEI = normalized negative enhancement integral

nMSD = normalized maximum signal decrease

* p<.05